Journal of Water Process Engineering 49 (2022) 103137

Contents lists available at ScienceDirect

Journal of Water Process Engineering

journal homepage: www.elsevier.com/locate/jwpe

# Development of a geometrical model for the determination of the average intensity in a flow-through UV-LED reactor and validation with biodosimetry and actinometry

Leonardo Romero-Martínez *, Javier Moreno-Andrés, Asunción Acevedo-Merino, Enrique Nebot

*Department of Environmental Technologies, Faculty of Marine and Environmental Sciences, INMAR - Marine Research Institute, CEIMAR - International Campus of Excellence of the Sea, University of Cadiz, Spain*

ARTICLE INFO

*Keywords:*
Ultraviolet disinfection
Light-emitting diodes
Bacterial inactivation kinetics
Actinometry
Biodosimetry

ABSTRACT

Ultraviolet (UV) treatment is widely used for water disinfection. The recent development and improvement of the light emitting diodes (LEDs) in the UVC range makes them an alternative to the traditional mercury vapor UV lamps in the middle or long term. Determining the UV intensity applied by a reactor is essential for evaluating its efficacy. Although doing so is relatively straightforward in simple laboratory reactors, such as a collimated beam reactor (CBR), its calculation for more complex devices, such as a flow-through reactor (FTR), requires indirect approaches. The objective in this study is determining the UV intensity in FTRs equipped with UV-C LEDs by utilizing indirect approaches such as the geometrical modeling of the intensity distribution, chemical actinometry, and biodosimetry using a CBR as a reference. With this method, the inactivation of four bacterial indicators in both the CBR and FTR have also been addressed. The three approaches that were used reported similar values of mean intensity with an average value of 0.86 mW $cm^{-2}$. Determining the mean intensity enabled calculating the UV doses that were applied to the target water and then determining the inactivation kinetics parameters. The UV dose that was necessary to achieve four-log reductions from the initial bacterial concentration ranged from 5.8 to 17.5 mJ $cm^{-2}$ depending on the target species. Additionally, the geometrical model developed in this study introduces new possibilities into the optimization of the reactor design.

## 1. Introduction

The use of ultraviolet (UV) irradiation has been increasing in the recent decades as a method to inactivate waterborne organisms [1–3]. UV is considered to be an effective treatment that avoids the use of chemical reagents and the formation of harmful disinfection byproducts [4]. The sources of germicidal UV radiation in the UVC range have traditionally been the low-pressure (LP) or medium-pressure (MP) mercury lamps. Although these lamps have high output power for germicidal radiation, they demonstrate several disadvantages such as the necessity of warming up, low energetic efficiency, relatively short lifetime, and the use of mercury in manufacturing that is harmful in the event of leakage or if the lamp breaks [5]. The recent development of UV light-emitting diode (UVC-LED) technology presumably poses the end of the use of mercury lamps for disinfection in the medium to long term. The current primary disadvantage of the UVC-LED as disinfection technology is its low output power; however, this issue is being addressed by research with promising advances [6]. On the other hand, UVC-LED shows several benefits regarding the traditional UV lamps such as less electric consumption, no necessity of a warming up period, longer lifetime, greater flexibility in the wavelengths of emission, and possibilities for configuration in a disinfection reactor.

To evaluate the inactivating efficacy of an UV reactor, it is necessary to obtain the inactivation curves (survival vs UV dose) that can be fitted to inactivation models and subsequently determine the inactivation kinetics parameters [7]. The mean UV dose that is applied is defined as the product of the reactor mean intensity ($I_m$) and the exposure time. Determining both factors depends on the reactor features. UV validation processes are based on collimated beam reactors (CBRs) because of their design, 2D, with collimated beams of light, parallel to each other and perpendicular to the surface of the reactor, which makes it easy to

* Corresponding author at: Department of Environmental Technologies, INMAR-Marine Research Institute, University of Cádiz, Campus Universitario Puerto Real, 11510 Puerto Real, Cádiz, Spain.

*E-mail addresses:* leonardo.romero@uca.es (L. Romero-Martínez), javier.moreno@uca.es (J. Moreno-Andrés), asuncion.acevedo@uca.es (A. Acevedo-Merino), enrique.nebot@uca.es (E. Nebot).

https://doi.org/10.1016/j.jwpe.2022.103137
Received 5 July 2022; Received in revised form 18 August 2022; Accepted 7 September 2022
Available online 18 September 2022

**Nomenclature**

| | |
|---|---|
| $P$ | output UV power |
| $r$ | distance between the center of coordinates and the point A |
| $T_W$ | water transmittance |
| $T_Q$ | quartz transmittance |
| $r_0$ | quartz sleeve radius |
| $q$ | quartz sleeve thickness |
| $\alpha$ | angle with respect to the perpendicular of the LED 1 |
| $\beta$ | angle with respect to the perpendicular of the LED 2 |
| $f(\alpha)$ | fourth order polynomial modeling the relative intensity with respect to the angle $\alpha$ |
| $f(\beta)$ | fourth order polynomial modeling the relative intensity with respect to the angle $\beta$ |
| $I_0$ | intensity at a distance $r$ from the LED without attenuation due to the medium |
| $I_i$ | intensity at a distance $r$ from the LED, attenuated by the quartz and water absorption |
| $r_1$ | distance between the LED 1 and the point A |
| $r_2$ | distance between the LED 2 and the point A |
| $z$ | distance between the LED 1 and the cross section containing the point A |
| $d$ | displacement between two adjacent rows of LEDs |
| $r_{01}$ | distance between the LED 1 and quartz sleeve |
| $r_{02}$ | distance between the LED 2 and quartz sleeve |
| $y_1$ | distance between the center of coordinates and the LED 1 |
| $x_2$ | distance between the center of coordinates and the LED 2 |
| $r_{S1}$ | distance between the LED 1 and the reactor shell |
| $r_{S2}$ | distance between the LED 2 and the reactor shell |
| $r_{F1}$ | distance between the reactor shell and the point A, in the direction connecting the LED 1 and the point A |
| $r_{F2}$ | distance between the reactor shell and the point A, in the direction connecting the LED 2 and the point A |
| $r_{T1}$ | total distance elapsed from the LED 1 until the reactor shell and back to the point A in the same direction |
| $r_{T2}$ | total distance elapsed from the LED 2 until the reactor shell and back to the point A in the same direction |
| $I_A$ | total intensity at the point A |
| $I_1$ | intensity due to the LED 1 |
| $I_2$ | intensity due to the LED 2 |
| $R$ | coefficient of reflection |
| $I_{R1}$ | intensity due to the LED 1 reflection in the reactor shell |
| $I_{R2}$ | intensity due to the LED 2 reflection in the reactor shell |
| $D$ | UV dose |
| $RED$ | reduction equivalent dose |
| $TRT$ | theoretical retention time |
| $N$ | cell concentration after irradiation |
| $N_0$ | initial cell concentration |
| $S$ | survival ($N/N_0$) |
| $S_0$ | survival in absence of UV irradiation, according to the model fitted |
| $k$ | inactivation rate in the log-linear range |
| $SL$ | shoulder length in log-linear + shoulder model |
| $S_{res}$ | asymptotic survival at high UV doses in log-linear + tail model |
| $RMSE$ | root mean square error |
| $D_n$ | UV dose required to achieve "n" log-reduction from the initial concentration |

characterize the light distribution in the reactor. CBRs allows determining $I_m$ directly by means of irradiance measurements, the morphometry of the reactor, and the water UV transmittance [8,9] and enables direct control of the exposure time. On the other hand, the most industrial applications require treating large volumes of water and then a flow-through reactor (FTR) becomes necessary. The challenge with FTRs is that the geometry is more complex, and therefore, the direct determination of $I_m$ is not possible as occurs in CBRs; therefore, it must be calculated by means of different approaches such as geometrical modeling, actinometry, and biodosimetry [10,11]. Diverse geometrical models of the UV intensity distribution have been developed for traditional UV Hg lamps and recently for LED lamps [12]. Whereas the intensity pattern in Hg lamps is homogeneous along the length of the lamp, the discrete nature of each LED as an individual source of radiation forces the intensity pattern to be heterogeneous and dependent on the position of each LED. Nonetheless, the information obtained through a theoretical approach such as the geometrical modeling must be validated experimentally. Chemical actinometry allows determining the photon flux in a reactor based on a photochemical reaction rate of which the quantum yield is known [13,14]. Biodosimetry is used to determine the UV intensity in complex reactors, such as FTRs, by means of comparing the inactivation level achieved with respect to a CBR with known intensity. In this case, the range of UV doses in which the biodosimetry is applicable depends on the UV resistance of the organisms, and it is usually affected by "shouldering" and "tailing" phenomena [7] as time intensity reciprocity may not always apply.

According to recent studies such as [11], two of the current challenges in UV-LED disinfection are the identification of appropriate target organisms for emerging waterborne pathogens and application scenarios as well as addressing the complex geometries for the model simulation that pose the UV-LEDs imply with respect to the conventional UV sources. USEPA recommends the model simulation to evaluate the reactor performance and the different operational conditions [7]. Models are divided in two main groups: mathematical models to simulate the optical field in the reactor and prediction of fluid field based the computational fluid dynamics. The emerging light sources such as UV-LEDs allows complex pattern in their configuration, which pose new challenges to the application of model simulation, with the aim of determining the optimum setup of the reactor for the maximum efficacy and the least consumption of resources. In this context, the objective in this study is to develop a geometrical model of UV irradiation distribution that allows determining the mean intensity in a UVC-LED flow-through reactor and optimizing its design parameters as well as to validate it with chemical actinometry and biodosimetry. Additionally, the efficacy of UV-LEDs on four bacterial indicators with different features regarding their UV resistance and interest in different fields have been obtained.

## 2. Material and methods

### 2.1. UV devices description

#### 2.1.1. Collimated beam reactor (CBR)

The CBR (Photolab LED275-0.01/300-0.03/365-1cb, APRIA Systems S.L., Spain) was equipped with a LED UV-C with power of 10.5 mW and emission wavelength between 265 and 285 nm, with maximum at 275 nm, and a collimator tube with collimator lens of 5.08 cm of diameter and focal length of 6 cm. The treatment was applied to samples in Petri dishes with a diameter of 55 mm and a capacity for 20 mL of target water. A magnetic stirrer with a volume of 0.25 mL was added to the Petri dish to ensure continuous stirring throughout irradiation. The sample surface was at 12.2 cm of the UV light source.

The UV dose that was applied was calculated as the product of the mean intensity and the exposure time [15]. The mean intensity for the CBR was determined according to the Bolton protocol spreadsheet available at https://www.iuva.org/Guidance-Documents [9]. This

protocol is based on the reactor morphometry, direct measurement of the irradiance at the center of the sample surface, and the water UV transmittance ($T_W$). Additionally, the protocol requires determining the Petri factor by means of direct irradiance measurements across the sample surface. The irradiance was measured with a radiometer (HD 2102.1, Delta OHM, Padova, Italy) that was equipped with a probe able to measure the UV-C and UV-B spectra (LP471UVBC, Delta OHM, Padova, Italy). $T_W$ at 275 nm of the target water was measured with a spectrophotometer (Jenway 7315; Staffordshire, UK) immediately prior to the sample irradiation.

### 2.1.2. Flow-through reactor (FTR)

The continuous flow UV device (Photolab LED275-0.4c, APRIA Systems S.L., Spain) consisted of an FTR mounted in a laboratory rig with hydraulic and electric systems. It was configured as a traditional annular reactor (Fig. 1) with the UV lamp in the center surrounded by a quartz sleeve with an external diameter of 40 mm, thickness of 1.5 mm, and UV quartz transmittance of 0.92. The UV lamp was constructed from metal with a squared cross section of 20 mm of side length. Each side contained a row of ten LEDs, comprising a total of 40 of them. Each row of LEDs was displaced at 5 mm with respect to the adjacent rows. The LEDs used in the FTR were the same than those used in the CBR, with output power of each LED was 10.5 mW and emission between 265 and 285 nm, with emission peak at 275 nm.

The FTR was mounted in a vertical position in a laboratory rig equipped with a 20 L reservoir, a peristaltic pump, and a set of valves that allowed establishing flow rates from 45 up to 200 L $h^{-1}$. The rig can be configured for operating as a continuous flow system with or without recirculation, and the reactor can also be isolated for operating as a batch reactor in closed vessels. According to the reactor morphometry, the irradiated volume is 0.361 mL. The *TRT* was determined as the quotient between the irradiated volume and the flow rate.

## 2.2. Geometrical modeling of mean intensity in the FTR

The intensity of the emitted radiation from a point focus such as an LED is scattered in void space according to the quotient between the LED power and the irradiated surface that corresponds to a hemisphere in the case of a single LED (Eq. 1).

$$I_0 = \frac{P}{2\pi r^2} \tag{1}$$

According to the LEDs' manufacturer provided information, the relationship between relative intensity and the angular displacement can be modeled as a fourth order polynomial for angles between −90 and 90° (Fig. 2). This function is known as f($\alpha$) and expresses the relative intensity with respect to the angle $\alpha$.

When radiation passes through a liquid medium, it is subsequently attenuated as a function of the transmittance of the irradiated medium and the distance travelled through such a medium; a factor calculating the attenuation due to the quartz sleeve was also included (Eq. 2).

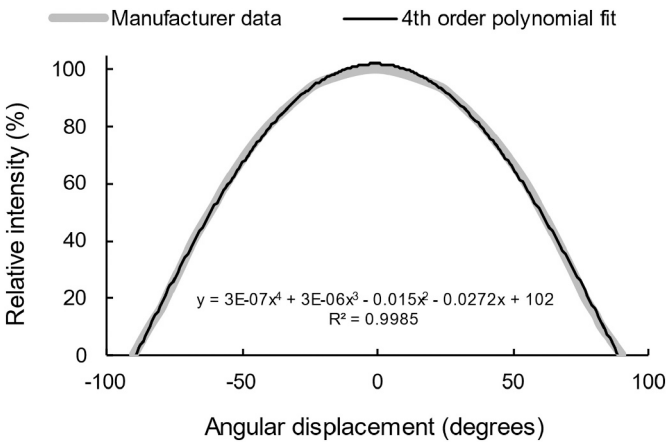


**Fig. 2.** Variation of the intensity with respect to the angle from the LED vertical, according to the manufacturer.

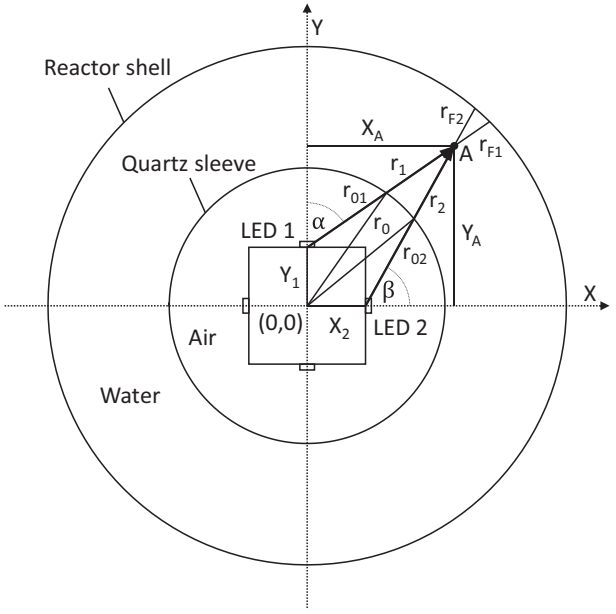


**Fig. 3.** Representation of the FTR cross section corresponding to the plane through LED 1 and LED 2, assuming absence of displacement between adjacent rows.

$$I_i = I_0 \cdot T_W^{(r-r_0)} \cdot T_Q^{q} \tag{2}$$

In the quadrangular arrangement of the LEDs, every point (A) of the

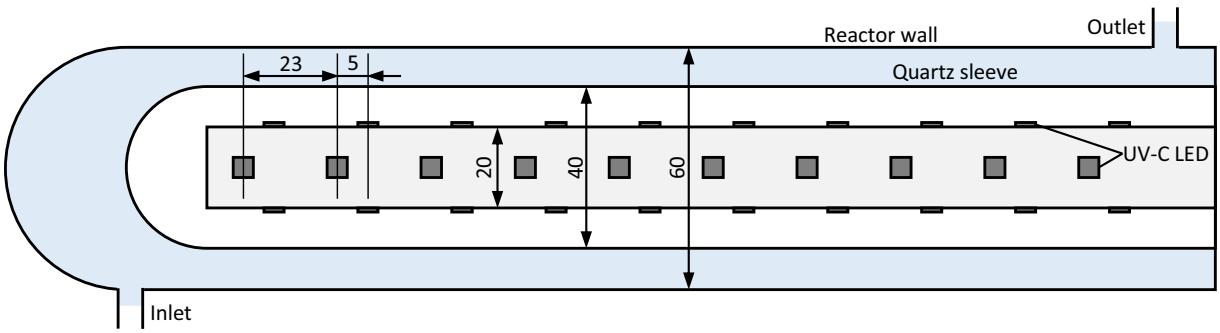


**Fig. 1.** Diagram of the FTR design. Measurements are in mm.

space in a cross section at a distance $z$ from the LED 1 can be illuminated by only two LEDs (Fig. 3), according to the relative intensity distribution (Fig. 2). Taking the center of the quadrangular prism as the origin of coordinates, $r_1$ and $r_2$ are the Euclidean distances from LED 1 (0, $y_1$, 0) and LED 2 ($x_2$, 0, 0) to point A ($x_A$, $y_A$, $z_A$), respectively. α and β are the angles that vectors $r_1$ and $r_2$ form with the perpendicular to the LED 1 and 2, respectively, in their plane of the cross section. $r_{01}$ and $r_{02}$ are the distances travelled between the LEDs and the quartz sleeve which is a space containing air in which the transmittance is considered as 1 and therefore the radiation is not absorbed. The intensity at point A will therefore be the sum of the intensity due to LED 1 and LED 2 (Eqs. 3 and 4):

$$I_1 = \frac{P}{2\,\pi\, r_1^2} T_W^{\,r_1 - r_{01}} \cdot T_Q^q \cdot f(\alpha) \tag{3}$$

$$I_2 = \frac{P}{2\,\pi\, r_2^2} T_W^{\,r_2 - r_{02}} \cdot T_Q^q \cdot f(\beta) \tag{4}$$

The distances $r_1$ and $r_2$ are calculated through the coordinates of each point and the position of each LED (Eqs. 5 and 6).

$$r_1 = \sqrt{x^2 + (y - y_1)^2 + z^2} \tag{5}$$

$$r_2 = \sqrt{(x - x_2)^2 + y^2 + (z - d)^2} \tag{6}$$

To calculate the segments $r_{01}$ and $r_{02}$, the triangles of sides ($r_{01}$, $r_0$, $y_1$) and ($r_{02}$, $r_0$, $x_2$) were solved with known angles ($\pi - \alpha$) and ($\pi - \beta$) through the cosine theorem solving for $r_{01}$ from the resulting second-degree polynomial (Eqs. 7–10). In this case, $\alpha$ and $\beta$ are expressed in radians. Resolution and inclusion of the dimension $z$ provide the path-length that the light travels in air medium (Eqs. 11 and 12).

$$r_0^2 = r_{01}^2 + y_1^2 - 2\, r_{01} \cdot y_1 \cdot cos\,(\pi - \alpha) \tag{7}$$

$$r_0^2 = r_{02}^2 + x_1^2 - 2\, r_{02} \cdot x_1 \cdot cos\,(\pi - \beta) \tag{8}$$

$$r_{01}^2 + y_1^2 - 2 \cdot r_{01} \cdot y_1 \cdot cos\,(\pi - \alpha) - r_0^2 = 0 \tag{9}$$

$$r_{02}^2 + x_2^2 - 2 \cdot r_{02} \cdot x_2 \cdot cos\,(\pi - \beta) - r_0^2 = 0 \tag{10}$$

$$r_{01} = \sqrt{\left(\frac{2 \cdot y_1 \cdot cos\,(\pi - \alpha) + \sqrt{4 \cdot y_1^2 \cdot cos^2\,(\pi - \alpha) - 4\,(y_1^2 - r_0^2)}}{2}\right)^2 + z^2} \tag{11}$$

$$r_{02} = \sqrt{\left(\frac{2 \cdot x_2 \cdot cos\,(\pi - \beta) + \sqrt{4 \cdot x_2^2 \cdot cos^2\,(\pi - \beta) - 4\,(x_2^2 - r_0^2)}}{2}\right)^2 + (z - d)^2} \tag{12}$$

As the inner surface of the reactor shell is reflective, it must be considered that part of the radiation that arrives on this surface will reflect and thus increase the UV intensity in each point of the bulk reactor. For estimating the intensity due to reflection in any point A, it must be considered that the radiation is attenuated through the travelled distance for the beam from the two nearest LEDs to the inner external surface and back to the point A (Eqs. 13 and 14).

$$r_{T1} = r_{S1} + r_{F1} \tag{13}$$

$$r_{T2} = r_{S2} + r_{F2} \tag{14}$$

The intensity in each point will be due to both the direct and the reflective irradiation (Eq. 15). The reflected radiation it is calculated according to Eqs. 16 and 17 for which $R$ is a reflection coefficient depending on the surface material.

$$I_A = I_1 + I_2 + I_{R1} + I_{R2} \tag{15}$$

$$I_{R1} = \frac{P}{2\,\pi\, r_{T1}^2} \cdot R \cdot T_W^{\,2 \cdot r_{S1} - r_1 - r_{01}} \cdot T_Q^q \cdot f(\alpha) \tag{16}$$

$$I_{R2} = \frac{P}{2\,\pi\, r_{T2}^2} \cdot R \cdot T_W^{\,2 \cdot r_{S2} - r_2 - r_{02}} \cdot T_Q^q \cdot f(\beta) \tag{17}$$

A matrix with 84 × 84 cells was developed in Microsoft Excel© in which $I_A$ was discretized for a grid of points belonging to one quadrant of the cross section of the irradiated volume, obtaining the mean and the standard deviation of the UV intensity in that cross section.

In opposition to the traditional mercury lamps, with homogeneous lengthwise distribution of the intensity, the point source of the LEDs emission causes the lengthwise intensity to be heterogeneous depending on the position of the LEDs with regard to the plane of the considered cross section. Using a Macro developed in Microsoft Excel©, the mean and standard deviation of the UV intensity was calculated for a series of cross sections at both sides from the LED 1 and LED 2. By adding the curves corresponding to every LED arranged in the lamp, the average intensity ($I_m$) of the reactor can be calculated by integrating the sum curve. Once the $I_m$ is known, the mean UV dose can be calculated as the product of $I_m$ and *TRT*.

The Supporting Information contains the Microsoft Excel spreadsheet to calculate the mean intensity according to the geometrical model developed in this study (Fig. 4). The spreadsheet requires input data including the output power for each individual LED, the percentage of total power set in the device, the number of LEDs per side of the support structure, the cross section length of the support structure, misalignment between adjacent rows of LEDs, distance between LEDs, thickness of the quartz sleeve, outer radius of the quartz sleeve, inner radius of the reactor shell, quartz transmittance (92 %, according to [16]), water transmittance, factor of reflectance of the reactor shell, and the water flow rate (not necessary for calculating $I_m$, but useful for calculating the UV dose). Based on the input data, the spreadsheet calculates $I_m$ and the maximum standard deviation and coefficient of variation of the intensity along the different cross sections used in the calculation; additionally, other useful parameters are calculated such as the irradiated volume, retention time, and UV dose for the introduced flow rate.

### 2.3. Chemical actinometry experiment

The chemical actinometry was performed at a high concentration of $H_2O_2$ according to [17] for determining the incident intensity ($I_0$). The initial $H_2O_2$ concentration was 32 mM. Accordingly, Eq. 18 (in which C is the concentration of the actinometer, $\Phi$ is the quantum yield, $L$ is the effective path of the radiation, and $\varepsilon$ is the extinction coefficient) can be simplified into Eq. 19 and thus determine $I_0$ [18]. The quantum yield ($\Phi$) for $H_2O_2$ at wavelength of 275 nm was 1.055 mol Einstein$^{-1}$ and was calculated by the interpolation of the data presented in [19].

$$-\frac{dC}{dt} = \Phi\, I_0 \left(1 - e^{-ln(10)\; L\; \varepsilon\; C}\right) \tag{18}$$

$$-\frac{dC}{dt} = \Phi\, I_0 \tag{19}$$

Due to the large *TRT* that is needed for a correct quantification of $H_2O_2$ extinction, the UV device was configured for operating as a batch reactor. The initial volume was 0.6 L of $H_2O_2$ solution at 32 mM that was prepared by adding the corresponding volume of $H_2O_2$ stock (30 % ultrapure, Scharlau) into distilled water. Throughout the experiment, a continuous air flow was pumped into the reactor in order to avoid heating the water, and the reactor content was continuously stirred with a magnetic stirrer. A 1 mL sample was extracted from the reactor every 5 min until a treatment time of 30 min was completed. The $H_2O_2$ concentration in samples was determined using the DIN 38402 H15 colorimetric method with titanium (IV) oxysulfate and measuring absorbance at 410 nm [20].

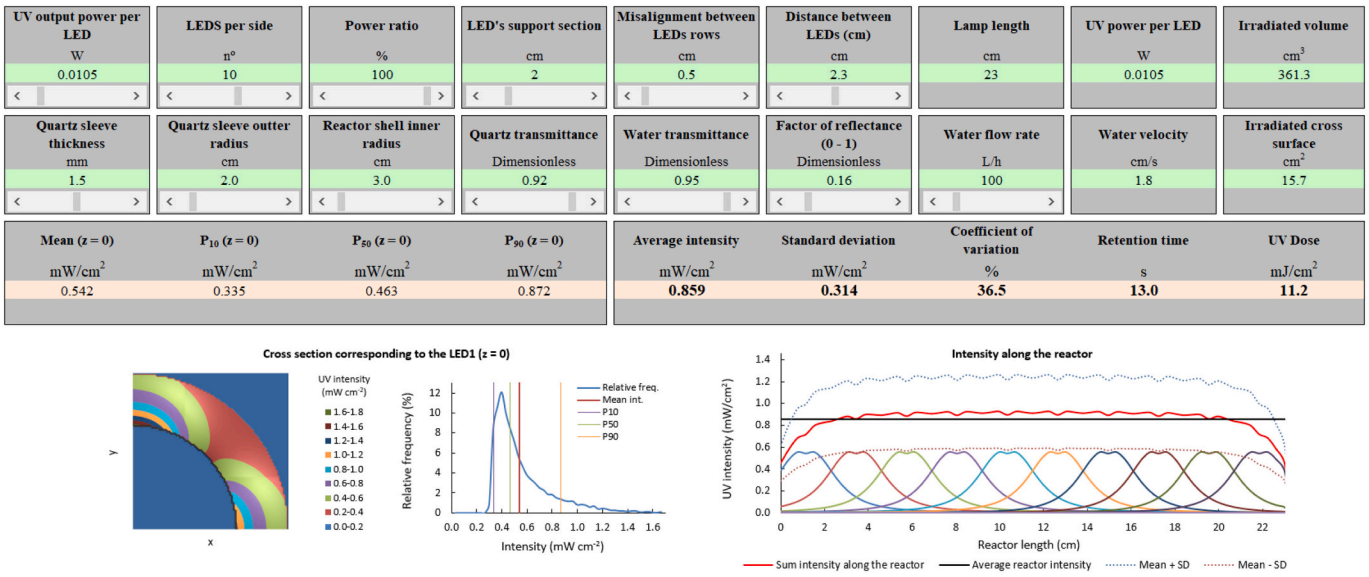


**Fig. 4.** Spreadsheet developed for determining the radiation distribution within the reactor and the mean intensity (available in Supporting Information).

The value of $I_0$ was determined according to Eq. 19; $I_m$ was then calculated according to Eq. 20 ($I_m$ is the mean intensity, $I_0$ is the incident intensity, $A_{275}$ is the absorbance at 275 nm, and $d$ is the light pathlength in the reactor) [7,13].

$$I_m = I_0 \frac{1 - 10^{-A_{275}\ d}}{A_{275}\ d\ ln(10)} \quad (20)$$

### 2.4. Biodosimetry and inactivation kinetics

#### 2.4.1. Microbiological strains and procedures

Four indicator organisms that are of interest in the treatment of water were tested: *Escherichia coli* (ATCC 8739), *Enterococcus faecalis* (ATCC 19433), vegetative *Bacillus subtilis* (ATCC 6633) and the seawater bacteria *Vibrio alginolyticus* (ATCC 17749). Lyophilized bacterial strains were acquired from the Spanish Type Culture Collection (CECT - University of Valencia, Spain). Strains were reactivated in an adequate culture broth: Tryptic Soy Broth (Scharlab, Barcelona, Spain) for *E. coli* and *B. subtilis*, Brain Heart Infusion Broth (Scharlab) for *E. faecalis* and Marine Broth (Scharlab) for *V. alginolyticus*. Organisms were incubated for 24 h at 37 °C in the case of the *E. coli*, *E. faecalis* and *B. subtilis* and at 30 °C for the *V. alginolyticus*. 1 mL of culture was then sub-cultured into fresh medium and incubated again for 24 h. Aliquots of 1 mL of the cultures were then placed into Eppendorf vials and centrifugated at 3000 rpm for ten minutes. The supernatant was removed, the pellet resuspended, and added with 1 mL of 50:50 glycerol-water solution. Vials were stored in a freezer at −20 °C. Two days before the experiment, the content from one vial was reactivated in the corresponding culture broth following the same sub-culturing procedure as that described for the lyophile. A maximum of three sub-culturing steps were done from one vial to ensure genetic stability of the culture. After incubation, the culture was centrifugated, the supernatant removed, and the pellet resuspended using the corresponding water matrix to obtain the bacterial inoculum. The water matrix was distilled water to which was added 1.25 mL of phosphate buffer at pH 7.20 per L of water in the cases of *E. coli*, *E. faecalis,* and *B. subtilis* and artificial seawater prepared by the addition of Instant Ocean® Sea Salt (Aquarium Systems, VA, USA) in distilled water, reaching a conductivity of 50 mS $cm^{-2}$ at 25 °C for the *V. alginolyticus*. The bacterial inoculum was then added into the experimental rig container with 20 L of water matrix in order to obtain the target water for the treatment. The inoculated water matrix was stored for 40 min prior to the experiment in order to allow the acclimation of the organisms and to discard those organisms from the experiment that did not survive the dilution in the water matrix. The average initial bacterial concentrations obtained were $1.32 \cdot 10^6$ CFU $mL^{-1}$ for *E. coli*, $2.23 \cdot 10^6$ CFU $mL^{-1}$ for *E. faecalis*, $4.45 \cdot 10^4$ CFU $mL^{-1}$ for *B. subtilis* and $1.61 \cdot 10^6$ CFU $mL^{-1}$ for *V. alginolyticus*. An aliquot of 200 mL of target water was drawn from the reservoir to be subjected to the CBR treatment and the remaining water to the FTR treatment.

After the treatment, samples were subjected to a ten-fold dilution and 0.45 μm membrane filtration and subsequently incubated in 55 mm diameter Petri dishes with the corresponding agar for determining the concentration of viable bacteria. *E. coli* was incubated using Micro-instant® Colinstant Chromogenic Agar (Scharlab) at 37 °C for 24 h; *E. faecalis* was incubated using Slanetz and Bartley Agar (Scharlab) with TTC indicator at 27 °C for 48 h; *B. subtilis* was incubated using Nutritive Agar (Scharlab) at 37 °C for 24 h; and *V. alginolyticus* was incubated using TCBS Agar (Scharlab) at 30 °C for 24 h. Colony forming units (CFU) were counted after the incubation, and plates with 20 up to 150 CFU were considered as valid for determining the bacterial concentration.

#### 2.4.2. Experimental procedure

Biodosimetry implies performing CBR and FTR experiments and then finding a correlation between them. For the CBR experiments, aliquots of 20 mL of inoculated water matrix were placed in a 55 mm Petri dish and then irradiated between 10 s and 25 min with continuous stirring. The UV dose applied to each sample was calculated using the Bolton et al. spreadsheet [9]. Water transmittance was measured using an HD 2102.1 radiometer that was equipped with a LP471UVBC probe (Delta OHM Srl, PD, Italy). Upon exposure, samples were subjected to membrane filtration and incubation as explained previously. At least three experiments were performed for every organism with different power settings in the reactor to cover the entire range of UV doses between 0 and 20 mJ $cm^{-2}$.

For the FTR experiments, 20 L of the inoculated water matrix were pumped once through the FTR at flow rates between 45 and 230 L $h^{-1}$, and 250 mL of samples were collected at the reactor outlet with sterile borosilicate flasks. Samples treated at low flow rates and thus subjected to high UV doses were taken in the first order to avoid contamination of the subsequent samples. After taking one sample, the flow rate was increased and measured, and then a water volume greater than the system volume was wasted to ensure correct UV exposure of the sample and avoiding mixtures with previous samples. Each reservoir with 20 L

allowed collecting five UV treated samples and the untreated control which created an experimental series. All samples in one experimental series were taken within 15 min and kept in the dark after collection. Once collected, all samples were subjected to membrane filtration and incubation procedures.

#### 2.4.3. Data treatment

Survival was calculated as the quotient between the CFU concentration in one treated sample and the mean CFU concentration in the control of the corresponding experimental series (Log ($S$) = $N_t$ / $N_0$). Using the CBR data belonging to the log-linear section of the dose-survival curve for every tested organism, the linear regression parameters between Log ($S$) and UV dose were determined. Regression parameters were used to calculate *RED* values based on the Log ($S$) data that was obtained using the FTR. Since the UV dose corresponds with the product of $I_m$ and *TRT*, *RED* values were represented against their corresponding *TRT*, and then $I_m$ was calculated as the curve slope, dismissing the values out of the linear range. For experiments using a lamp power below 100 %, *TRT* was multiplied by the power percentage. Once the UV doses could be calculated for both the CBR and FTR, the dose-survival curves for each tested organism were subsequently modeled according to microbiological inactivation models using the GInaFit tool for MS Excel [21]. Inactivation parameters that were determined by modeling were used to calculate the $D_n$ values which allows comparing the inactivation performance for each reactor on each organism.

## 3. Results and discussion

### 3.1. Determination of $I_m$ of the FTR with actinometry and biodosimetry

#### 3.1.1. Chemical actinometry

In the chemical actinometry, the $H_2O_2$ concentration decreased with time according to a linear relationship with a slope equal to $-1.29 \cdot 10^{-6}$ M $s^{-1}$ (Fig. 5). According to Eq. 19, $I_0$ could be calculated as $1.22 \cdot 10^{-6}$ Einstein $L^{-1}$ $s^{-1}$. $I_0$ was then calculated in units of mW $cm^{-2}$ according to the photon energy and the experimental setup. The photon energy at wavelength of 275 nm can be calculated as $4.35 \cdot 10^5$ J $Einstein^{-1}$, thus obtaining $I_0$ equal to 0.531 W $L^{-1}$. Since six aliquots of sample were taken from the reactor, the average sample volume was 0.57 L, and $I_0$ was calculated as 0.303 W. Considering the outer bond of the quartz sleeve as the emission area with 289.03 $cm^2$, $I_0$ was equal to 1.047 ± 0.096 mW $cm^{-2}$. The mean intensity ($I_m$) in the reactor can be calculated from $I_0$, absorbance at 275 nm, and the radiation pathlength (Eq. 20). As the mean $T_w$ at 275 nm in inactivation experiments was 0.95, this value has been used as the reference, obtaining the $I_m$ value of 1.020 ± 0.094 mW $cm^{-2}$.

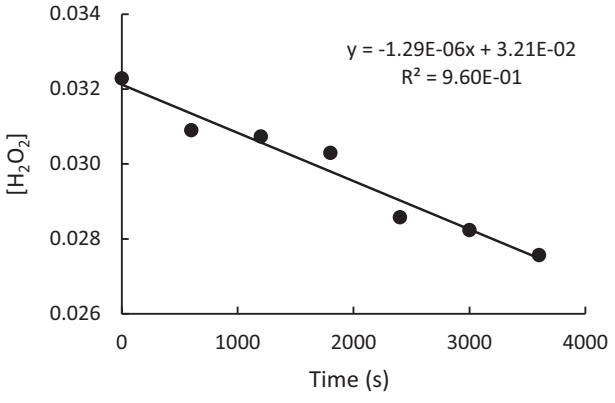


**Fig. 5.** Variation of the $H_2O_2$ concentration with the irradiation time in actinometry.

#### 3.1.2. Biodosimetry

Inactivation curves that were obtained with the CBR indicated that *E. coli*, *E. faecalis,* and *B. subtilis* demonstrated a shoulder region at low UV doses whereas *V. alginolyticus* showed tailing at high UV doses (Fig. 6). The range of linearity in inactivation curves defines the range of UV doses for which the biodosimetry can be applied for each organism. In organisms that follow the log-linear + shoulder model, the application range starts at the beginning of the log-linear section and ends at the maximum experimental dose whereas, in the organisms that followed log-linear + tail model, the application ranges run from a UV dose equal to zero up to the end of the log-linear section (Table 1). Within the linearity range, Log ($S$) correlated with the UV dose with $R^2$ values >0.9, with significant intercept value, indicating the existence of an initial shoulder section except for *V. alginolyticus* and a significant slope with values according to the UV resistance by the tested organism.

Regression parameters obtained for the CBR data were used to calculate the *RED* values corresponding to every Log ($S$) data obtained using the FTR. *RED* values were represented against their corresponding *TRT*, multiplied by the power percentage if the reactor was set at a power below 100 % (Fig. 7a), and $I_m$ was calculated as the curve slope for each organism. $I_m$ values ranged from 0.78 and 0.84 mW $cm^{-2}$ (Fig. 7b), although the analysis with Further ANOVA for Variables in the Order Fitted (Statgraphics Centurion XVI, ver. 16.1.03) reported an absence of statistical differences ($p$ = 0.508) between slopes from the four tested organisms. Taking into account the $I_m$ values obtained with actinometry and biodosimetry, the mean value of $I_m$ for the FTR set at full power and $T_W$ of 0.95 ± 0.02 was determined as 0.86 ± 0.09 mW $cm^{-2}$.

#### 3.1.3. Determination of $I_m$ of the FTR through geometrical modeling

The distribution of the UV radiation within the FTR was examined using the Excel spreadsheet developed and included in Supporting Information. Taking the cross section that coincides with one LED as a reference, it is remarkable that the intensity distribution is highly irregular through the cross section with values between 0.2 and 1.8 mW $cm^{-2}$, obviously with the highest values at the proximity of the LEDs. This implies that the coefficient of variation of the intensity reached values up to 39 %, thus the different organisms all passing through the reactor at the same time are exposed to different actual UV doses. However, inactivation data obtained with the FTR do not show greater dispersion in comparison with the data obtained with the CBR, indicating a good representativity of the calculated mean UV dose. $I_m$ calculated for the FTR through geometrical modeling assuming $T_W$ equal to 0.95, and the lack of reflection was 0.80 mW $cm^{-2}$. However, using a reflectance factor for the reactor wall equal to 16 %, $I_m$ matched with the mean value of 0.86 mW $cm^{-2}$ that was obtained with actinometry and biodosimetry (Fig. 7).

### 3.2. Comparison of bacterial inactivation kinetics obtained with the CBR and FTR

Once the $I_m$ for both the CBR and FTR were known, the inactivation curves for the different tested organisms were obtained by representing Log ($S$) against the applied UV dose (Fig. 6). The data obtained with the FTR fitted with the same inactivation models as those obtained with the CBR. The inactivation of *E. coli*, *E. faecalis* and *B. subtilis* followed the log-linear + shoulder model (Eq. 21) whereas it followed the log-linear + tail model (Eq. 22) for that of the *V. alginolyticus* [22].

$$S = S_0 \cdot \frac{e^{-k \cdot D} \cdot e^{k \cdot SL}}{1 + e^{-k \cdot D} \cdot (e^{k \cdot SL} - 1)} \quad (21)$$

$$S = (S_0 - S_{res}) \cdot e^{-k \cdot D} + S_{res} \quad (22)$$

The reciprocity in the UV dose calculation, depending on either applying low intensity for a longer time (CBR) or high intensity for a

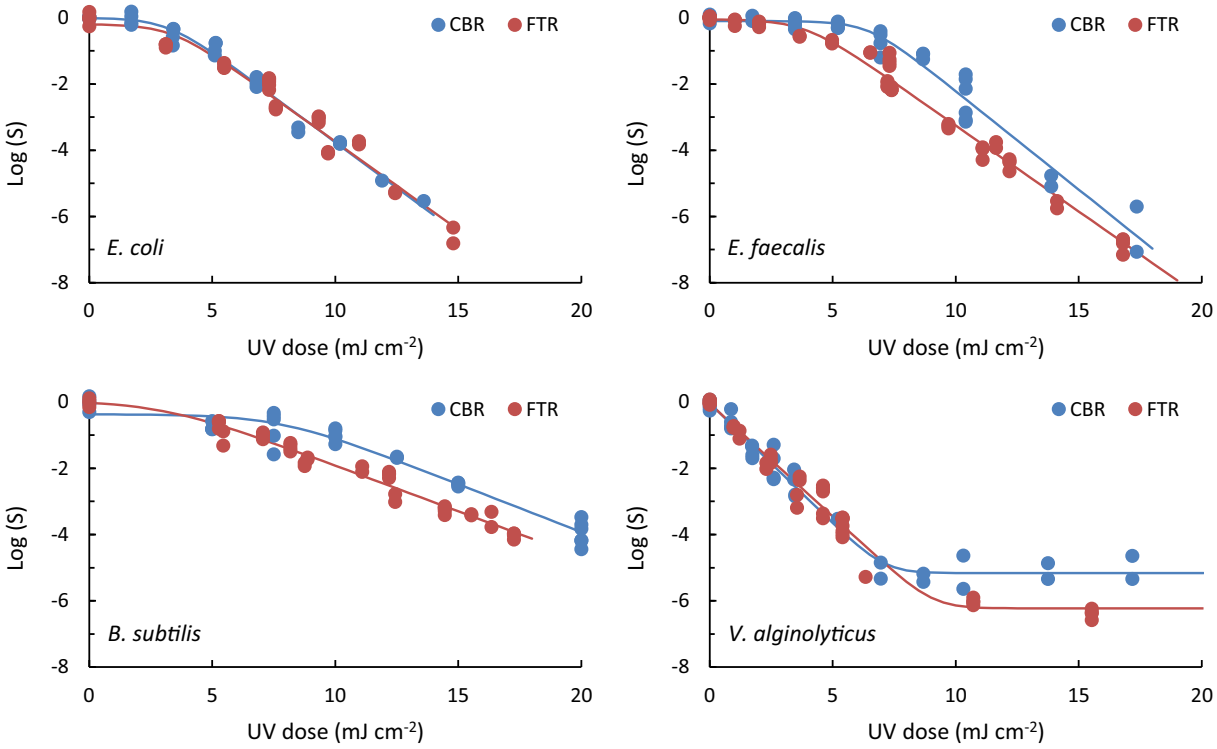


**Fig. 6.** Inactivation curves of the four tested organisms using the collimated beam reactor (CBR) and the flow-through reactor (FTR). Symbols correspond to collected data and lines represent the inactivation model fitting the data.

**Table 1**
Linear regression parameters for the linearity sections of the inactivation curves obtained using the collimated beam reactor.

| Organism | Linearity range (mJ cm$^{-2}$) | Intercept ± SE (*p*-value) | Slope ± SE (p-value) (cm$^2$ mJ$^{-1}$) | $R^2$ | n |
|---|---|---|---|---|---|
| *E. coli* | 5–14 | 1.85 ± 0.21 (<0.001) | −0.562 ± 0.025 (<0.001) | 0.977 | 14 |
| *E. faecalis* | 7–17 | 3.49 ± 0.45 (<0.001) | −0.577 ± 0.041 (<0.001) | 0.930 | 17 |
| *B. subtilis* | 10–20 | 1.99 ± 0.21 (<0.001) | −0.298 ± 0.014 (<0.001) | 0.969 | 17 |
| *V. alginolyticus* | 0–7 | −0.05 ± 0.08 (0.509) | −0.710 ± 0.027 (<0.001) | 0.964 | 27 |

shorter time (FTR), was assessed based on the similarity between kinetics parameters that were obtained with both reactors (Table 2). In the case of *E. coli*, both reactors induced the same inactivation effect. For *E. faecalis* and *B. subtilis*, inactivation curves obtained with both reactors showed similar *k* for each organism, although the shoulder region was longer in the case of the CBR. This lack of reciprocity at low UV doses has been reported by different authors [23–25], and it is attributed to the competence of repairing processes with the inactivation. In the case of *V. alginolyticus*, values of *k* were almost similar for both reactors, although the inactivation reached with the FTR was one order of magnitude greater in comparison with the CBR according to the values of Log ($S_{res}$). Tailing phenomenon has commonly been observed in the inactivation of bacteria and other organisms such as viruses, protozoa, and microalgae that are subjected to UV or other physical and chemical treatments [26–29]. In certain cases, tailing does not appear in the inactivation curve, although its presence is assumed beyond the

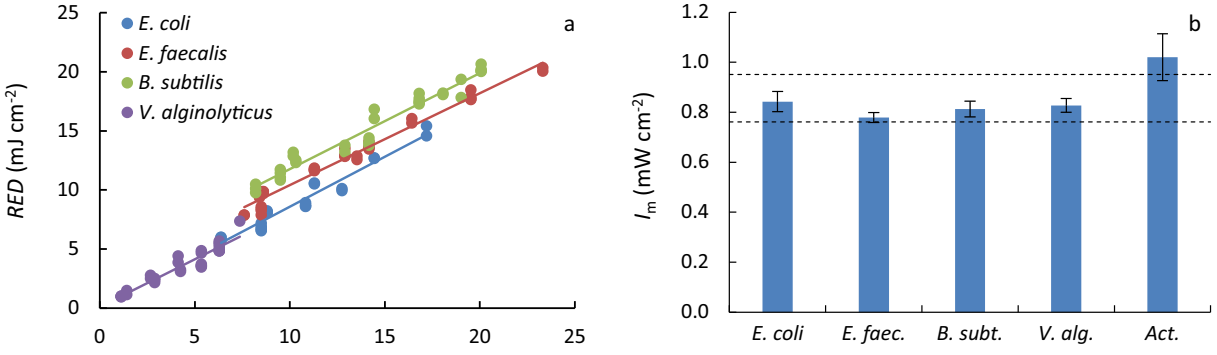


**Fig. 7.** a: Representation of the reduction equivalent dose (*RED*) with respect to the product of the theoretical retention time (*TRT*) and the set power percentage of the LEDs (*p*). b: Mean intensity determined with biodosimetry for the different organisms tested and actinometry.

**Table 2**
Inactivation kinetics parameters obtained for the four tested organisms using both collimated beam and flow-through reactors.

| Organism | Reactor | Model | *SL* (mJ cm$^{-2}$) | *k* (cm$^2$ mJ$^{-1}$) | Log ($S_{res}$) | $D_4$ (mJ cm$^{-2}$) | $R^2$ |
|---|---|---|---|---|---|---|---|
| *E. coli* | CBR | L-L + S | 3.2 ± 0.3 | 1.27 ± 0.05 | – | 10.4 ± 0.7 | 0.985 |
| | FTR | L-L + S | 3.3 ± 0.4 | 1.22 ± 0.06 | – | 10.5 ± 1.1 | 0.965 |
| *E. faecalis* | CBR | L-L + S | 6.4 ± 0.4 | 1.37 ± 0.07 | – | 13.0 ± 0.9 | 0.962 |
| | FTR | L-L + S | 3.8 ± 0.2 | 1.20 ± 0.02 | – | 11.4 ± 0.5 | 0.989 |
| *B. subtilis* | CBR | L-L + S | 7.7 ± 0.9 | 0.67 ± 0.05 | – | 20.3 ± 2.3 | 0.945 |
| | FTR | L-L + S | 3.2 ± 0.6 | 0.64 ± 0.02 | – | 17.5 ± 1.5 | 0.972 |
| *V. alginolyticus* | CBR | L-L + T | – | 1.67 ± 0.08 | −5.17 ± 0.11 | 5.5 ± 0.4 | 0.976 |
| | FTR | L-L + T | – | 1.57 ± 0.05 | −6.23 ± 0.11 | 5.8 ± 0.3 | 0.980 |

experimental range of applied UV doses [30]. The reason for tailing has been a matter of debate and explained as being due to a subpopulation of resistant organisms, the presence of suspended particles and flocs, hydraulics and closeness to the detection limit, among others [31–33]. Tailing was observed in *V. alginolyticus* treated with both the CBR and FTR at bacterial concentrations considerably greater than the detection limit and at relatively low UV doses of approximately 6 mJ cm$^{-2}$; therefore, it can be attributed to the presence of a subpopulation with higher resistance to UV treatment. The high reciprocity between inactivation data obtained with the CBR and FTR makes both *E. coli* and *V. alginolyticus* an appropriate biodosimeter respectively for higher (5–20 mJ cm$^{-2}$) and lower UV dose range (0–7 mJ cm$^{-2}$).

The existence of a shoulder region in the inactivation curves and the fact that the various organisms followed different inactivation models, the values of *k* cannot be directly compared for assessing bacterial UV resistance. In this sense, the UV resistance by the different organisms was evaluated using $D_4$, that is, the UV dose necessary to achieve 4-log reductions from the initial concentration. According to their respective $D_4$, the less resistant organism was *V. alginolyticus* followed by *E. coli*, then *E. faecalis* and, finally, *B. subtilis* as the most resistant species. The data obtained in this study match with different studies that state that, for the same UV dose, emission at wavelength of 275 nm by LED lamps is more effective for bacterial inactivation in comparison with the emission at 254 nm of the traditional LP Hg lamps [34–36]. Results also revealed a reduction of the UV resistance of *E. faecalis* when treated with 275 nm LEDs, showing $D_4$ values that were much more similar to *E. coli* in comparison with studies that used LP Hg lamps [35] that showed greater differences between $D_4$ values for both species. It is remarkable that, although the FTR reached 4 log-reductions of vegetative cell of *B. subtilis*, it presumably will not reach the inactivation of *B. subtilis* spores required for drinking water purification as it is much more resistant than vegetative cells [33]. Nevertheless, it is observed that the UV resistance is dependent on the specific bacterial strain that was tested; even using the same strain, the values of $D_4$ show high variability between studies [37,38]. This fact indicates that there is still great heterogeneity in the methods used by the different authors to calculate UV doses and bacterial survival.

### 3.3. Behavior of the geometrical model and use for the design of reactors

The geometrical model developed in this work allows the quantitative study of the radiation distribution across and along the reactor which may be used to optimize the reactor design. The study of the radiation distribution involves different variables; among them, the most important one that defines the UV dose applied to the treated organisms is the mean intensity. However, it was observed that, taking the cross section that passes through one LED as a reference, the intensity across the illuminated surface ranges from 0.29 up to 1.66 mW cm$^{-2}$. In addition, the radiation distribution differs clearly from a normal distribution curve (Fig. 4) with most of the cross surface receiving less than the mean intensity. In this sense, the relationship between the percentiles 10, 50, and 90 are a better approach rather than the standard deviation for assessing the radiation distribution through the cross section of the reactor.

The radius of the reactor shell is one of the major parameters involved in the optimization of the reactor design. The radius defines the value of $I_m$ in such a way that it decreases as the pathlength through the water increases (Fig. 8a) since the larger area is exposed to low intensity farther away from the LEDs. However, the exposed volume increases with the radius and thus also the exposure time and the UV dose (Fig. 8b). This continuous increase of the mean UV dose with the reactor shell is suitable only for high $T_W$ values close to 95 %. Therefore, the optimum reactor radius depends on the type of water for which it was designed. In the treatment of clean water with high transmittance, an excessively narrow reactor may cause the wasting of high amounts of energy. On the other hand, for treating water with low transmittance, increasing the reactor radius does not effectively increase the mean UV dose, and more area within the reactor is exposed to low intensity that may contribute to a failure in the treatment efficacy.

The flexibility in the LEDs disposition allows the optimization of the reactor efficacy without increasing the number of active lamps. This flexibility makes it possible to displace the different rows of LEDs with

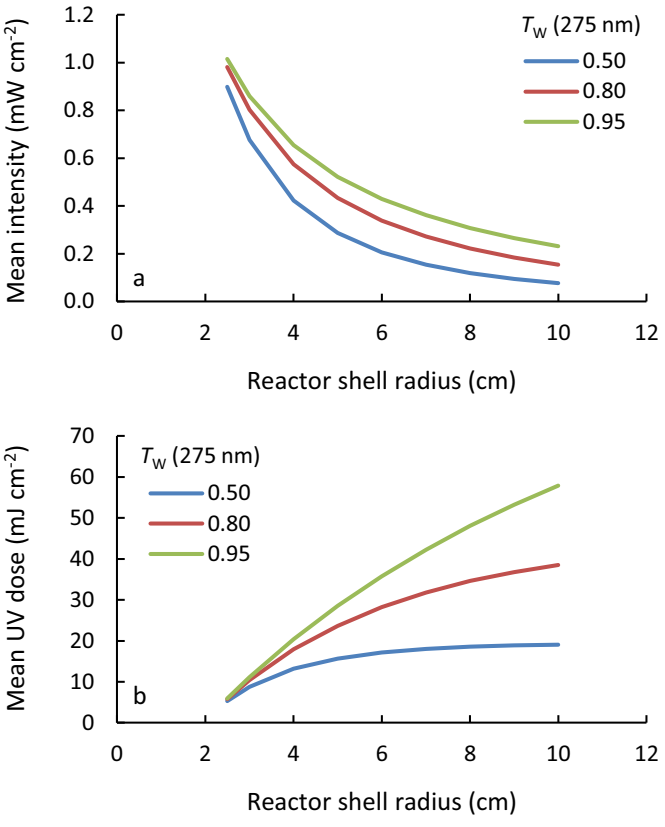


**Fig. 8.** Variation of the mean intensity (a) and mean UV dose (b) in the plane corresponding to one LED ($z$ = 0 cm), for different values of water transmittance.

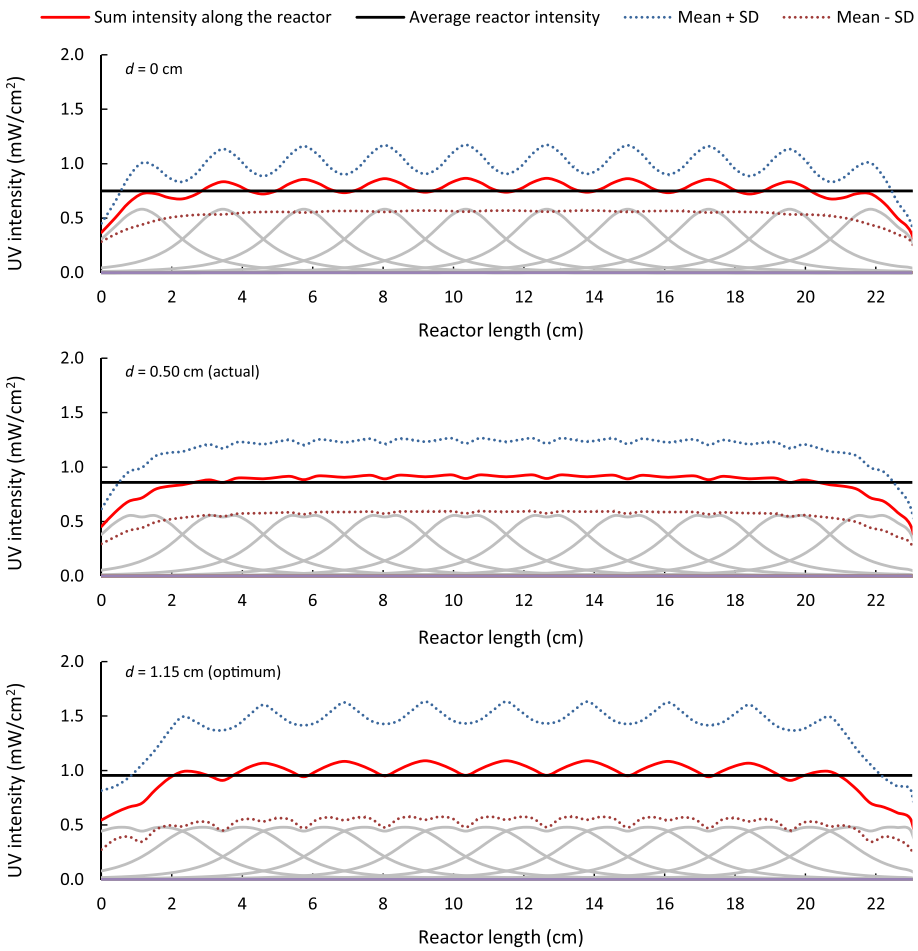


**Fig. 9.** Variation of the mean intensity of the reactor with respect to the displacement between adjacent LED rows ($d$). Grey lines represent the intensity by the different LED lamps along the reactor.

respect to the adjacent rows which allows a better distribution of the intensity along the reactor (Fig. 9). $I_m$ increases from 0.75 mW cm$^{-2}$ in the case of the four LEDs on the same plane ($d = 0$ cm) up to 0.95 mW cm$^{-2}$ in the case of displacing two rows of LEDs into the middle point between two adjacent LEDs from the other rows, that is, $d = 1.15$, with a separation between LEDs of the same row of 2.30 cm.

The use of UV-LEDs flow-through reactors is being investigated for practical applications such as drink water purification, waste water reuse and prevention of diseases and exogenous species spreading from aquaculture effluents and ballast water. In this context, the processes of photoreactivation and dark repair, which contribute to the regrowth of the treated organisms, needs to be addressed [39,40]. Similarly, UV-LEDs can be used as the activator in advanced oxidation processes for the degradation of organic pollutants [41]. The reactor optimization that enables the model simulation developed in this study may improve the water treatment for these different practical applications that use.

## 4. Conclusions

The complex geometry of the flow-through UV reactors, used commonly for the water disinfection in applications such as drink water purification, wastewater reuse, aquaculture effluents disinfection and ballast water treatment, makes necessary the use of indirect approaches for determining the UV intensity. The mean intensity of a UV-LED flow-through reactor for water disinfection was determined utilizing three approaches: geometrical modeling of the radiation distribution within the irradiated water volume, chemical actinometry, and biodosimetry. They reported a similar value of mean intensity, indicating the suitability of the geometrical model developed in this study which is provided along with this article as an Excel spreadsheet in the Supporting Information. The geometrical model reported significant heterogeneity in the UV intensity distribution within the reactor due to the individualized character of the LED lamps. However, the bacterial inactivation data that was obtained did not show a dispersion greater than that observed using a collimated beam reactor. This indicates that the heterogeneity in the intensity distribution is not a concern for the water disinfection. Due to the flexibility of the LED lamps regarding their disposition within a reactor, the geometrical model of radiation distribution may enable the optimization of the designing of reactors to maximize the UV dose applied to the target water.

The four organisms tested in this study as biodosimeter showed different ranges of UV dose in which the biodosimetry was feasible and different time-intensity reciprocity. Biodosimetry with *E. coli* was suitable between 5 and 17 mJ cm$^{-2}$, and the inactivation was similar when treated with high UV intensity for a short time and with low UV intensity for a longer time. On the other hand, *V. alginolyticus* was suitable for a UV dose range between 0 and 7 mJ cm$^{-2}$ with appropriate time-intensity reciprocity. The suitability of *E. faecalis* and *B. subtilis* was limited because of the lack of time-intensity reciprocity since the treatment with high intensity for short time reduced the shoulder section in the inactivation curves of both organisms.

## Declaration of competing interest

The authors declare that they have no known competing financial interests or personal relationships that could have appeared to influence

the work reported in this paper.

## Data availability

Data will be made available on request.

## Acknowledgements

This work has been co-funded by the 2014–2020 ERDF Operational Programme and by the Department of Economy, Knowledge, Business and University of the Regional Government of Andalusia (Spain). Projects Ref.: FEDER-UCA18-108023 and FEDER-UCA18-105151. J. Moreno-Andrés acknowledges Grant IJC2020-042741-I funded by MCIN/AEI/10.13039/501100011033 and by the European Union NextGenerationEU/PRTR.

## Appendix A. Supplementary data

Supporting Information contains the Excel spreadsheet with the geometrical model for the UV radiation distribution within the reactor. It can be used for determining the mean UV intensity and doses for different reactor configurations. Supplementary data to this article can be found online at doi: https://doi.org/10.1016/j.jwpe.2022.103137

## References

[1] M. Abbaszadegan, M.N. Hasan, C.P. Gerba, P.F. Roessler, B.R. Wilson, R. Kuennen, E. Van Dellen, The disinfection efficacy of a point-of-use water treatment system against bacterial, viral and protozoan waterborne pathogens, Water Res. 31 (1997) 574–582, https://doi.org/10.1016/S0043-1354(96)00263-1.

[2] S. Li, Y. Tao, X.M. Zhan, G.H. Dao, H.Y. Hu, UV-C irradiation for harmful algal blooms control: a literature review on effectiveness, mechanisms, influencing factors and facilities, Sci. Total Environ. 723 (2020), 137986, https://doi.org/10.1016/j.scitotenv.2020.137986.

[3] J.L. Darby, K.E. Snider, G. Tchobanoglous, Ultraviolet disinfection for wastewater reclamation and reuse subject to restrictive standards, Water Environ. Res. 65 (1993) 169–180, https://doi.org/10.2175/WER.65.2.10.

[4] Y. Penru, A.R. Guastalli, S. Esplugas, S. Baig, Application of UV and UV/H2O2 to seawater: disinfection and natural organic matter removal, J. Photochem. Photobiol. A Chem. 233 (2012) 40–45, https://doi.org/10.1016/j.jphotochem.2012.02.017.

[5] S. Schalk, V. Adam, E. Arnold, K. Brieden, UV-lamps for disinfection and advanced oxidation – lamp types, technologies and applications, IUVA News 8 (2006) 32–37. http://iuva.org/sites/default/files/member/news/IUVA_news/Vol08/Issue1/SchalkArticleIUVANewsVol8No1.pdf.

[6] T.C. Hsu, Y.T. Teng, Y.W. Yeh, X. Fan, K.H. Chu, S.H. Lin, K.K. Yeh, P.T. Lee, Y. Lin, Z. Chen, T. Wu, H.C. Kuo, Perspectives on UVC LED: its progress and application, Photonics 8 (2021) 196, https://doi.org/10.3390/photonics8060196.

[7] USEPA, Ultraviolet Disinfection Guidance Manual for the Final Long Term 2 Enhanced Surface Water Treatment Rule, Tech. Report, US Environ. Prot. Agency, Off. Water, 2006.

[8] J.R. Bolton, K.G. Linden, Standardization of methods for fluence (UV Dose) determination in bench-scale UV experiments, J. Environ. Eng. 129 (2003) 209–215, https://doi.org/10.1061/(ASCE)0733-9372(2003)129:3(209).

[9] J.R. Bolton, S.E. Beck, K.G. Linden, Protocol for the determination of fluence (UV dose) using a low-pressure or low-pressure high-output UV lamp in benchscale collimated beam ultraviolet experiments, IUVA News 17 (2015) 11–16.

[10] S. Jin, A.A. Mofidi, K.G. Linden, Polychromatic UV fluence measurement using chemical actinometry, biodosimetry, and mathematical techniques, J. Environ. Eng. 132 (2006) 831–841.

[11] Z. Sun, M. Li, W. Li, Z. Qiang, A review of the fluence determination methods for UV reactors: ensuring the reliability of UV disinfection, Chemosphere 286 (2022), 131488, https://doi.org/10.1016/j.chemosphere.2021.131488.

[12] M. Martín-Sómer, C. Pablos, R. van Grieken, J. Marugán, Influence of light distribution on the performance of photocatalytic reactors: LED vs mercury lamps, Appl. Catal. B Environ. 215 (2017) 1–7, https://doi.org/10.1016/j.apcatb.2017.05.048.

[13] P. Jarvis, O. Autin, E.H. Goslan, F. Hassard, Application of ultraviolet light-emitting diodes (UV-LED) to full-scale drinking-water disinfection, Water 11 (2019) 1894.

[14] C.G. Hatchard, C.A. Parker, A new sensitive chemical actinometer - II. Potassium ferrioxalate as a standard chemical actinometer, Proc. R. Soc. London. Ser. A. Math. Phys. Sci. 235 (1956) 518–536, https://doi.org/10.1098/rspa.1956.0102.

[15] USEPA, Design Manual: Municipal Wastewater Disinfection. EPA/625/1-86/021, U.S. Environmental Protection Agency, Cincinnati, Ohio, 1986.

[16] I.W. Wait, E.R. Blatchley, Model of radiation transmittance by inorganic fouling on UV reactor lamp sleeves, Water Environ. Res. 82 (2010) 2272–2278, https://doi.org/10.2175/106143010x12681059116491.

[17] F.J. Beltran, M. Gonzalez, F.J. Rivas, J. Jaramillo, Application of photochemical reactor models to UV irradiation of trichloroethylene in water, Chemosphere 31 (1995) 2873–2885.

[18] A. Leifer, The Kinetics of Environmental Aquatic Photochemistry: Theory and Practice, Am. Chem. Soc. York, 1988.

[19] S. Goldstein, D. Aschengrau, Y. Diamant, J. Rabani, Photolysis of aqueous H2O2: quantum yield and applications for polychromatic UV actinometry in photoreactors, Environ. Sci. Technol. 41 (2007) 7486–7490, https://doi.org/10.1021/es071379t.

[20] G.M. Eisenberg, Colorimetric determination of hydrogen peroxide, Ind. Eng. Chem. Anal. Ed. 15 (1943) 327–328, https://doi.org/10.1021/i560117a011.

[21] A.H. Geeraerd, V.P. Valdramidis, J.F. Van Impe, GInaFiT, a freeware tool to assess non-log-linear microbial survivor curves, Int. J. Food Microbiol. 102 (2005) 95–105, https://doi.org/10.1016/j.ijfoodmicro.2004.11.038.

[22] A.H. Geeraerd, C.H. Herremans, J.F. Van Impe, Structural model requirements to describe microbial inactivation during a mild heat treatment, Int. J. Food Microbiol. 59 (2000) 185–209, https://doi.org/10.1016/S0168-1605(00)00362-7.

[23] R. Sommer, T. Haider, A. Cabaj, W. Pribil, M. Lhotsky, Time dose reciprocity in UV disinfection of water, Water Sci. Technol. 38 (1998) 145–150, https://doi.org/10.1016/S0273-1223(98)00816-6.

[24] R.B. Setlow, P.A. Swenson, W.L. Carrier, Thymine dimers and inhibition of DNA synthesis by ultraviolet irradiation of cells, Science 142 (1963) 1464–1466, https://doi.org/10.1126/science.142.3598.1464.

[25] C. Bowker, A. Sain, M. Shatalov, J. Ducoste, Microbial UV fluence-response assessment using a novel UV-LED collimated beam system, Water Res. 45 (2011) 2011–2019, https://doi.org/10.1016/j.watres.2010.12.005.

[26] K. Oguma, R. Kita, H. Sakai, M. Murakami, S. Takizawa, Application of UV light emitting diodes to batch and flow-through water disinfection systems, Desalination 328 (2013) 24–30, https://doi.org/10.1016/j.desal.2013.08.014.

[27] T.J. Nieuwstad, A.H. Havelaar, The kinetics of batch ultraviolet inactivation of Bacteriophage MS2 and microbiological calibration of an ultraviolet pilot plant, J. Environ. Sci. Health Part A Environ. Sci. Eng. Toxicol. 29 (1994) 1993–2007, https://doi.org/10.1080/10934529409376160.

[28] T. Sigstam, A. Rohatschek, Q. Zhong, M. Brennecke, T. Kohn, On the cause of the tailing phenomenon during virus disinfection by chlorine dioxide, Water Res. 48 (2014) 82–89, https://doi.org/10.1016/j.watres.2013.09.023.

[29] L. Romero-Martínez, I. Rivas-Zaballos, J. Moreno-Andrés, I. Moreno-Garrido, A. Acevedo-Merino, E. Nebot, Improving the microalgae inactivating efficacy of ultraviolet ballast water treatment in combination with hydrogen peroxide or peroxymonosulfate salt, Mar. Pollut. Bull. 162 (2021), 111886, https://doi.org/10.1016/j.marpolbul.2020.111886.

[30] L. Romero-Martínez, I. Rivas-Zaballos, J. Moreno-Andrés, I. Moreno-Garrido, A. Acevedo-Merino, E. Nebot, Effect of the length of dark storage following ultraviolet irradiation of Tetraselmis suecica and its implications for ballast water management, Sci. Total Environ. 711 (2020), 134611, https://doi.org/10.1016/j.scitotenv.2019.134611.

[31] T.C. Tan, Y. Azimi, R.R. Farnood, Tailing propensity in the ultraviolet disinfection of trickling filter and activated sludgewastewater treatment processes, Water Sci. Technol. 76 (2017) 623–632, https://doi.org/10.2166/wst.2017.242.

[32] E. Carré, J. Pérot, V. Jauzein, M. Lopez-Ferber, Impact of suspended particles on UV disinfection of activated-sludge effluent with the aim of reclamation, J. Water Process Eng. 22 (2018) 87–93, https://doi.org/10.1016/j.jwpe.2018.01.016.

[33] W.A.M. Hijnen, E.F. Beerendonk, G.J. Medema, Inactivation credit of UV radiation for viruses, bacteria and protozoan (oo)cysts in water: a review, Water Res. 40 (2006) 3–22, https://doi.org/10.1016/j.watres.2005.10.030.

[34] A. Chevremont, A. Farnet, M. Sergent, B. Coulomb, J. Boudenne, Multivariate optimization of fecal bioindicator inactivation by coupling UV-A and UV-C LEDs, Desalination 285 (2012) 219–225, https://doi.org/10.1016/j.desal.2011.10.006.

[35] L. Romero-Martínez, J. Moreno-Andrés, A. Acevedo-Merino, E. Nebot, Improvement of ballast water disinfection using a photocatalytic (UV-C + TiO2) flow-through reactor for saltwater treatment, J. Chem. Technol. Biotechnol. 89 (2014) 1203–1210, https://doi.org/10.1002/jctb.4385.

[36] K.A. Sholtes, K. Lowe, G.W. Walters, M.D. Sobsey, K.G. Linden, L.M. Casanova, Comparison of ultraviolet light-emitting diodes and low-pressure mercury-arc lamps for disinfection of water, Environ. Technol. 37 (2016) 2183–2188, https://doi.org/10.1080/09593330.2016.1144798.

[37] G. Chevrefils, É. Caron, H. Wright, G. Sakamoto, UV dose required to achieve incremental log inactivation of bacteria, protozoa and viruses, IUVA News 8 (2006) 38–45.

[38] K. Song, M. Mohseni, F. Taghipour, Application of ultraviolet light-emitting diodes (UV-LEDs) for water disinfection: a review, Water Res. 94 (2016) 341–349, https://doi.org/10.1016/j.watres.2016.03.003.

[39] P.O. Nyangaresi, Y. Qin, G. Chen, B. Zhang, Y. Lu, L. Shen, Comparison of the performance of pulsed and continuous UVC-LED irradiation in the inactivation of bacteria, Water Res. 157 (2019) 218–227, https://doi.org/10.1016/j.watres.2019.03.080.

[40] P.O. Nyangaresi, Y. Qin, G. Chen, B. Zhang, Y. Lu, L. Shen, Effects of single and combined UV-LEDs on inactivation and subsequent reactivation of E. coli in water disinfection, Water Res. 147 (2018) 331–341, https://doi.org/10.1016/j.watres.2018.10.014.

[41] G. Matafonova, V. Batoev, Recent advances in application of UV light-emitting diodes for degrading organic pollutants in water through advanced oxidation processes: a review, Water Res. 132 (2018) 177–189, https://doi.org/10.1016/j.watres.2017.12.079.